the representative structural candidates formed in the early stages of reduction of the TiO_2 (110) surface.

Four schematics in each structural model are shown: (110) plan-view, [001] projection, [1$\bar{1}$0] projection, and a bird's-eye view of the Ti interstitial coordination polyhedra. From the [001] projection, the reconstructed Ti atoms (Fig. 3, light blue) are viewed to occupy the same interstitial sites in the two models. However, from the [1$\bar{1}$0] projection, we can distinguish the two models by the positioning of the Ti interstitials along the [001] direction. In the [1$\bar{1}$0] projected models, Ti interstitials are positioned on top of Ti-only columns (*iv* sites) in the Onishi-Iwasawa model, whereas they are on top of Ti-O columns (*ih* sites) in the Park *et al*. model. The present [1$\bar{1}$0] projected HVEM and HAADF-STEM images show that the Ti interstitials are found on top of Ti-O columns. In all observations, our results directly evidence the formation of Ti interstitials in the *ih* sites under the present reducing condition, which is consistent with the Park *et al*. model but not with the Onishi-Iwasawa model.

It has been theoretically predicted that the above two models are energetically favorable structures (*10*, *12*). However, the fundamental difference in the two models is the stoichiometry of the surface: O is more deficient in the Park *et al*. model than in the Onishi-Iwasawa model. As shown in the schematics, the Ti interstitials are octahedrally coordinated to O in the two models, but the O atom at one apex of the O octahedra is absent (one Ti-O dangling bond is present) in the Park *et al*. model. However, if we remove the topmost O atoms (Fig. 3, yellow) from the Onishi-Iwasawa model to equalize the surface stoichiometry, two Ti-O dangling bonds would be introduced to the Ti interstitials because these O atoms lie on the equatorial plane of the O octahedra. Thus, simple dangling bond considerations suggest that the Ti interstitials in the *ih* sites should be energetically more favorable under the progressive reduction, which is consistent with our experimental findings.

Our observations show that interstitial Ti atoms (in *ih* sites) are actually involved in the reconstruction of TiO_2 (110) surfaces. The distance between proximate *ih* and *iv* sites is less than 1.5 Å along the [001] direction, but the present direct atomic-resolution images distinguish the two interstitial sites on the surface. These results not only provide an atomic-scale cornerstone for complex surface reconstructions in TiO_2, they also open up new possibilities for characterizing the atomic-scale structure and chemistry of oxide surfaces. Recently, Ti interstitials near the TiO_2 (110) surface region have been proposed to be responsible for the defect state in the band gap (*24*), although O vacancies have been thought to be the key for many years. The ability to directly see interstitial atoms at surfaces should substantially assist our understanding of surface structures and, hence, properties of TiO_2 and other oxide materials. Direct atomic-scale imaging with recent advanced EM is a powerful method for unravelling complex atomic structures of oxide surfaces.

References and Notes

1. V. E. Henrich, P. A. Cox, *The Surface Science of Metal Oxides* (Cambridge Univ. Press, Cambridge, 1994).
2. U. Diebold, *Surf. Sci. Rep.* **48**, 53 (2003).
3. D. S. Deak, *Mater. Sci. Technol.* **23**, 127 (2007).
4. J. M. Cowley, *Prog. Surf. Sci.* **21**, 209 (1986).
5. A. N. Chiaramonti, L. D. Marks, *J. Mater. Res.* **20**, 1619 (2005).
6. S. Ii *et al*., *Appl. Surf. Sci.* **241**, 68 (2005).
7. M. Bowker, *Curr. Opin. Solid State Mater. Sci.* **10**, 153 (2006).
8. H. Onishi, Y. Iwasawa, *Surf. Sci.* **313**, L783 (1994).
9. H. Onishi, Y. Iwasawa, *Phys. Rev. Lett.* **76**, 791 (1996).
10. K. T. Park, M. H. Pan, V. Meunier, E. W. Plummer, *Phys. Rev. Lett.* **96**, 226105 (2006).
11. S. D. Elliott, S. P. Bates, *Phys. Chem. Chem. Phys.* **3**, 1954 (2001).
12. S. D. Elliott, S. P. Bates, *Phys. Rev. B* **65**, 245415 (2002).
13. M. Blanco-Rey *et al*., *Phys. Rev. Lett.* **96**, 055502 (2006).
14. K. T. Park, M. Pan, V. Meunier, E. W. Plummer, *Phys. Rev. B* **75**, 245415 (2007).
15. M. Blanco-Rey *et al*., *Phys. Rev. B* **75**, 081402 (2007).
16. Y. Lu, B. Jaeckel, B. A. Parkinson, *Langmuir* **22**, 4472 (2006).
17. R. Nakamura *et al*., *J. Phys. Chem. B* **109**, 1648 (2005).
18. Materials and methods are available as supporting material on *Science* Online.
19. D. J. Smith, M. R. McCartney, L. A. Bursill, *Ultramicroscopy* **23**, 299 (1987).
20. M. R. McCartney, D. J. Smith, *Surf. Sci.* **250**, 169 (1991).
21. M. L. Knotek, P. J. Feibelman, *Phys. Rev. Lett.* **40**, 964 (1978).
22. R. D. Ramsier, J. T. Yates Jr., *Surf. Sci. Rep.* **12**, 243 (1991).
23. S. J. Pennycook, D. E. Jesson, *Ultramicroscopy* **37**, 14 (1991).
24. S. Wendt *et al*., *Science* **320**, 1755 (2008).

25. We thank H. Tsunakawa for assistance with HVEM observations. This work was supported in part by the Grant-in-Aid for Scientific Research on Priority Areas Nano Materials Science for Atomic-scale Modification 474 from the Ministry of Education, Culture, Sports and Technology. N.S. acknowledges support from PRESTO, the Japan Science and Technology Agency, and the Industrial Technology Research Grant Program in 2007 from the New Energy and Industrial Technology Development Organization. S.D.F. is supported as a Japanese Society for the Promotion of Science fellow.

Supporting Online Material

www.sciencemag.org/cgi/content/full/322/5901/570/DC1
Materials and Methods
Figs. S1 to S4
References

25 August 2008; accepted 12 September 2008
10.1126/science.1165044

The Extent of Non–Born-Oppenheimer Coupling in the Reaction of Cl(^2P) with *para*-H_2

Xingan Wang,[1] Wenrui Dong,[1] Chunlei Xiao,[1] Li Che,[1] Zefeng Ren,[1] Dongxu Dai,[1] Xiuyan Wang,[1] Piergiorgio Casavecchia,[1]* Xueming Yang,[1]† Bin Jiang,[2] Daiqian Xie,[2,3]† Zhigang Sun,[1,4] Soo-Y. Lee,[4] Dong H. Zhang,[1]† Hans-Joachim Werner,[5] Millard H. Alexander[6]†

Elementary triatomic reactions offer a compelling test of our understanding of the extent of electron-nuclear coupling in chemical reactions, which is neglected in the widely applied Born-Oppenheimer (BO) approximation. The BO approximation predicts that in reactions between chlorine (Cl) atoms and molecular hydrogen, the excited spin-orbit state (Cl*) should not participate to a notable extent. We report molecular beam experiments, based on hydrogen-atom Rydberg tagging detection, that reveal only a minor role of Cl*. These results are in excellent agreement with fully quantum-reactive scattering calculations based on two sets of ab initio potential energy surfaces. This study resolves a previous disagreement between theory and experiment and confirms our ability to simulate accurately chemical reactions on multiple potential energy surfaces.

For more than 150 years, the reaction of chlorine atoms with molecular hydrogen, $Cl(^2P) + H_2 \rightarrow HCl + H$, has been one of the most widely studied elementary chemical reactions (*1*–*3*). In particular, investigations of this reaction laid the framework for the development of transition-state theory (*4*). Recently, this reaction (*2*, *5*–*8*), as well as the reaction of F with H_2 (*9*–*11*), have become testing grounds for improving the depth and accuracy of our understanding of how quantum mechanics is manifested in chemical reactivity.

The Cl atom is a free radical, with an unfilled p shell, which imparts an electronic directionality to the atom. Only one of the three possible orientations leads, over a substantial barrier, to products (*5*, *12*). The other two orientations are nonreactive at low to moderate energies (Fig. 1). The interaction between the orbital and spin angular momenta of the atom results in two possible spin-orbit states, separated energetically by ~2.5 kcal/mol of energy (880 cm^{-1}). The dependence of the reactive potential energy surfaces (PESs) on the orientation of the p shell then manifests itself in a differing reactivity for the two spin-orbit states of the atom.

The understanding of collisions between atoms and molecules is vastly simplified by the Born-Oppenheimer (BO) approximation, which states that nuclear motion will occur on PESs that correspond to the energies of the rapidly rearranging electrons as a function of the positions of the more slowly moving nuclei. Thus, a particular electronic energy state of the reactants will evolve along a

single PES. In the case of the Cl + H_2 reaction, the excited spin-orbit state will react only if the BO approximation is broken during the reaction, which then allows the excited spin-orbit reactants to transfer from a nonreactive PES to the reactive PES, by means of what is called a "nonadiabatic transition" (*13*). This process is illustrated schematically in Fig. 1.

The overall applicability of the BO approximation to chemical reactions has been established by a large number of experimental studies (*3*, *14*). More specifically, in the case of the analogous reaction of F with D_2, Yang, Alexander, Werner, and their co-workers have shown (*11*) that the reactivity of the excited spin-orbit state of the F atom, compared to that of the ground spin-orbit state, is small except at very low collision energies, where the barrier limits reaction of the ground spin-orbit state. Here, molecular-beam experimental measurements agreed quantitatively with predictions of fully quantum calculations based on the accurate ab initio PESs for the FD_2 system determined by Li, Werner, and co-workers (*15*).

A natural extension would be to the Cl + H_2 reaction. Because of the significant increase in the reaction barrier [8.45 kcal/mol for Cl + H_2 (*16*) as compared to 1.63 kcal/mol for F + H_2 (*17*), without including the atomic spin-orbit splitting], the reaction cross section will be much smaller, so that experimental investigation of Cl + H_2 is a greater challenge. Quantum-scattering studies, similar to those done for F + H_2/D_2, predicted that the excited spin-orbit state of Cl will be even more unreactive than that of F, because of the larger spin-orbit splitting in the heavier Cl atom (*5*, *12*). However, contrary to the predictions of theory, an experimental molecular-beam study of the Cl + H_2 reaction by means of Doppler-selected time-of-flight (TOF) detection of the H-atom product suggested that reactivity of the excited spin-orbit state becomes increasingly dominant as the collision energy increases (*18*, *19*).

Other experiments have been designed to resolve this disagreement (*8*, *7*, *20*). Crossed–molecular beam measurements of differential cross sections for the Cl + H_2 reaction by Casavecchia and co-workers by means of mass-spectrometric detection of the HCl product suggested that the excited spin-orbit state played only a minor role (*7*). However, the experimental resolution was insufficient to separate unambiguously products formed by reaction of Cl* from those formed by Cl. Recently, Neumark and co-workers (*8*) used photodetachment spectroscopy of the ClH_2^- anion to probe the extent of non-BO coupling in the region of the ClH_2 PES where this coupling is most likely to occur. Neumark's experiments, and the analysis of the accompanying theoretical calculations (*21*), indicate that the breakdown in the BO approximation is small.

Having achieved high precision in the comparison of theory and experiment for the F + D_2 reaction (*11*), we applied the same strategy to the Cl + H_2 reaction. As discussed above, a particular challenge is the much smaller cross section for the latter reaction, due to the higher reaction barrier. We report here a high-resolution, crossed–molecular beam study of the Cl + H_2 reaction in which we make use of the H-atom Rydberg tagging method (*22*). We concentrated on low collision energies (E_c = 4 to 6 kcal/mol), where nonadiabatic effects are expected to be most pronounced (*5*, *12*). Because the barrier to the Cl + H_2 reaction, corrected for zero-point energy, is ~5.5 kcal/mol (*23*), quantum-mechanical tunneling will contribute appreciably to the reaction at the collision energies considered here.

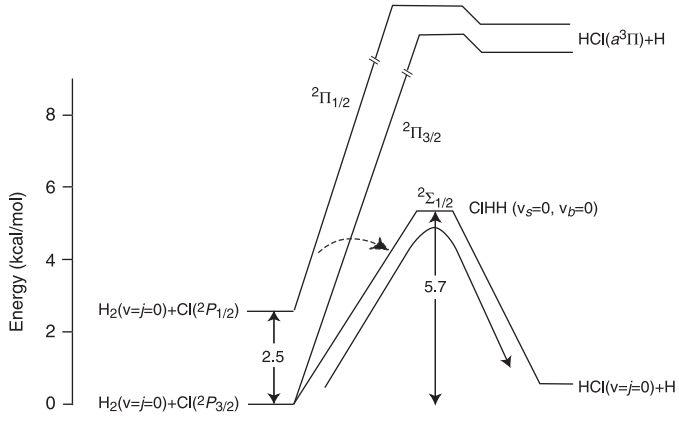

Fig. 1. Relative energies (to scale) for the Cl/Cl* + H_2 reaction, after inclusion of the spin-orbit splitting, with a schematic representation of the three ClH_2 electronically adiabatic PESs, labeled for collinear geometry. The vibrational zero-point energy (for reactants, products, and at the barrier) has been included. The PESs for the two Π states correlate, in the product arrangement, with HCl($a^3\Pi$) + H, which lies at least 150 kcal/mol above the Cl($^2P_{3/2}$) + H_2 asymptote. Consequently, the position of this asymptote is not drawn to scale. Reaction of Cl($^2P_{3/2}$) is BO-allowed and can proceed along the lowest PES (shown schematically by the solid arrow). However, for the excited spin-orbit state to react, a nonadiabatic "hop" (shown schematically by the dashed arrow) must occur from an excited PES to the lowest PES.

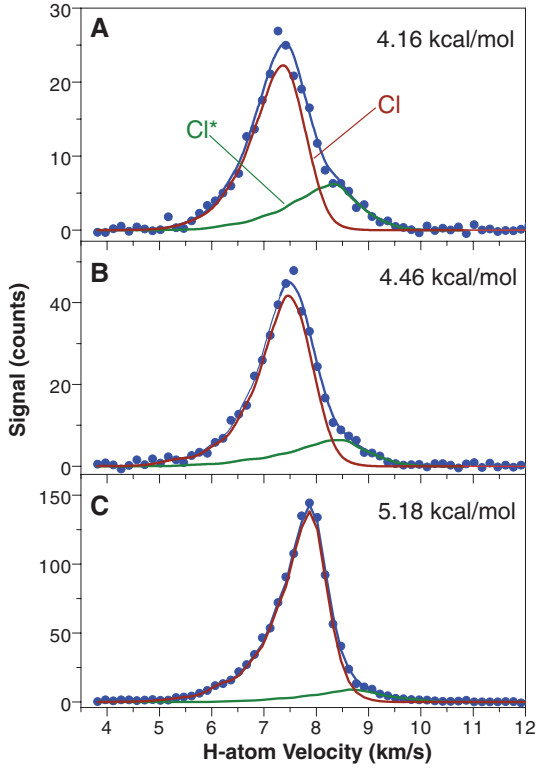

Fig. 2. Velocity spectra of the H-atom product from the Cl($^2P_{3/2}$)/Cl*($^2P_{1/2}$) + H_2 reaction in the backward direction at collision energies of (**A**) 4.16 kcal/mol, (**B**) 4.46 kcal/mol, and (**C**) 5.18 kcal/mol. In these spectra, the solid blue circles are the experimental results. To fit the experimental spectra, we used two components, corresponding to reaction of Cl and Cl*. As described in more detail in the SOM (*25*), we used the fitting procedure described in our F/F* + D_2 work (*11*). The blue curve shows the overall fit to the experimental velocity spectra and is the sum of the Cl component (red curve) and the Cl* component (green curve). From the simulations, it is apparent that the faster component, which corresponds to reaction of Cl*, makes a smaller contribution as the collision energy increases.

[1]State Key Laboratory of Molecular Reaction Dynamics, Dalian Institute of Chemical Physics, Chinese Academy of Sciences, Dalian, Liaoning 116023, People's Republic of China. [2]Institute of Theoretical and Computational Chemistry, Key Laboratory of Mesoscopic Chemistry of Ministry of Education, School of Chemistry and Chemical Engineering, Nanjing University, Nanjing 210093, People's Republic of China. [3]Division of Chemistry and Biological Chemistry, School of Physical and Mathematical Sciences, Nanyang Technological University, Singapore 637371, Singapore. [4]School of Physical and Mathematical Sciences, Nanyang Technological University, Singapore 637371, Singapore. [5]Institute für Theoretische Chemie, Universität Stuttgart, Pfaffenwaldring 55, D-70569 Stuttgart, Germany. [6]Department of Chemistry and Biochemistry and Institute for Physical Sciences and Technology, University of Maryland, College Park, MD 20742–2021, USA.

*Present address: Dipartimento di Chimica, Università di Perugia, 06123 Perugia, Italy.

†To whom correspondence should be addressed. E-mail: xmyang@dicp.ac.cn (X.Y.), dqxie@mail.nju.edu.cn (D.X.), zhangdh@dicp.ac.cn (D.H.Z.), and mha@umd.edu (M.H.A.)

Our experimental apparatus has been described previously (*10*, *24*, *25*). Briefly, we generated a doubly skimmed Cl-atom beam by expanding a mixture of 5% Cl_2/95% He through a two-stage discharge. We determined the Cl:Cl* ratio in the beam to be 3.3, by using 2+1 resonance-enhanced multiphoton ionization (REMPI). This ratio is similar to the ratio in the earlier experimental scheme of Liu and co-workers (*18*, *19*). Measurement of this ratio made it possible for us to extract the relative reactive cross sections of Cl* compared to Cl.

The *p*-H_2 was made by passing *n*-H_2 gas through a column filled with an *o-p* conversion catalyst cooled to about 20 K. The pure *p*-H_2 was expanded through a pulsed nozzle at room temperature. We estimate the rotational temperature of the emergent H_2 beam to be 140 K, at which point 89% is cooled to the lowest ($j = 0$) rotational state. The H-atom product from the Cl reaction with *p*-H_2 was detected with the H-atom Rydberg tagging technique (*25*).

TOF spectra of the H-atom products from the Cl/Cl* + *p*-H_2 reaction (with an intial Cl:Cl* ratio of 3.3) were measured at a range of laboratory angles varied in ~10° intervals. These TOF spectra were then converted to velocity spectra of the H-atom product. For scattering in the backward direction (H products rebounding opposite to the direction of the initial H_2 beam), Fig. 2 shows three typical H-atom velocity spectra at E_c = 4.16, 4.46, and 5.18 kcal/mol. The velocity spectra, which are proportional to the HCl product intensity at various laboratory scattering angles, were then simulated, as described in the Supporting Online Material (SOM) (*25*), to obtain the relative differential cross sections (DCSs) in the center-of-mass (CM) frame for the Cl and Cl* reactions. With this, and the experimentally determined Cl:Cl* population ratio in the beam, we can determine the relative reactivity of Cl and Cl* with H_2.

The accompanying theoretical simulations entailed time-independent, fully quantum-reactive scattering calculations, based on the time-independent formalism of Alexander, Manolopoulos, Werner and colleagues (*26*, *27*). This treatment of the dynamics includes explicitly four diabatic PESs; three of these correspond to the three possible orientations of the singly filled Cl 3p orbital with respect to the H_2, whereas the fourth diabatic PES represents the coupling between the two PESs of *A′* reflection symmetry (*23*, *26*). In addition, we include two coordinate-dependent spin-orbit constants, as well as Coriolis coupling between the four internal angular momenta (electronic spin, electronic orbital, diatomic rotational, and overall tumbling).

To determine differential reactive cross sections, we extended standard expressions to treat a system with multiple internal angular momenta (*27*). Our calculations were based on the Capecchi-Werner (CW) set of PESs (*23*) that were used in our previous work (*5*, *8*, *7*, *12*, *21*). In addition, to rule out any inaccuracies introduced by the method used to fit the CW ab initio points, we used a second set of diabatic PESs, which are a fit to additional multireference, configuration-interaction calculations by Jiang and Xie (JX). The methodology (in particular, the determination of the diabatic PESs) and computer codes used by JX were identical to those used by CW (*23*, *26*, *28*), but with some differences in the technicalities of the calculations, the number of points determined, and the way in which the ab initio points were fit (*25*).

Figure S3 displays the calculated DCSs for a collision energy of 4.75 kcal/mol, predicted by simulations on both sets of PESs. For reaction of both Cl and Cl*, the DCSs are smooth and peaked in the backward direction, identical in qualitative appearance to figures 2 to 4 of (*27*). The calculated DCSs for the BO-allowed reaction of Cl are nearly identical to those determined in earlier reactive scattering calculations in which the spin-orbit Hamiltonian and the electronic anisotropy of the Cl atom were ignored (*2*, *29*). The DCSs for reaction of the excited SO state are less backward peaked, which is consistent with the 2.5-kcal/mol increase in the total available energy due to the spin-orbit energy of Cl*. Figure 3 compares the CW DCSs at 4.75 kcal/mol, summed over accessible HCl rotational levels, with the experimentally determined CM angular distributions. The agreement between experiment and theory is excellent, although theory predicts a slightly broader distribution for the Cl* channel.

To assess the relative reactivity of the Cl and Cl* reactants, we examined the dependence on collision energy of the DCSs in the backward direction in the center-of-mass frame, where they are the largest. Figure 4 compares the experimentally determined, and theoretically predicted, DCSs in the backward direction ($\theta_{CM} = 180°$) for the Cl and Cl* reactions for collision energies ranging between 4 and 6 kcal/mol. For all colli-

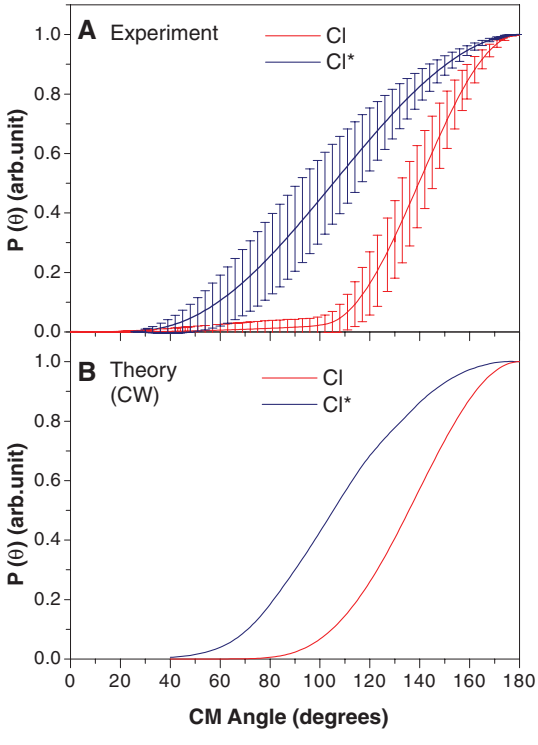

Fig. 3. Angular distributions in the CM system at a collision energy of 4.75 kcal/mol for reaction of Cl($^2P_{3/2}$) (red curve) and Cl*($^2P_{1/2}$) (blue curve) + *p*-H_2, as determined by our crossed–molecular beam experiments (**A**) and by fully quantum simulations on the CW set of PESs (**B**). In both cases, angular distributions were determined for the $j = 0$ and 2 rotational levels of H_2 with fractional populations corresponding to a Boltzmann distribution at $T = 140$ K. The error bars in (A) indicate the range of error in the experimentally derived CM angular distribution $P(\theta)$. The evaluation of the error bars of the experimental data is discussed in the SOM (*25*).

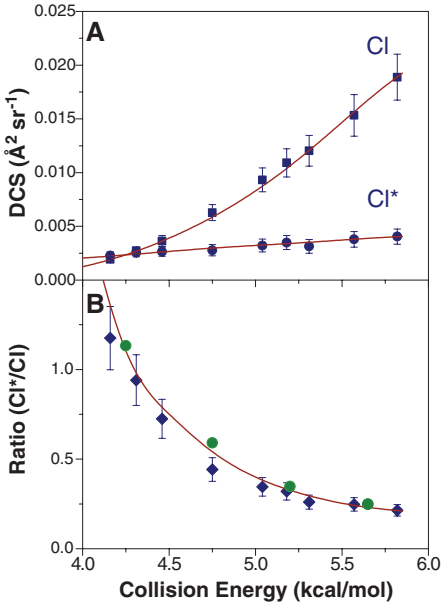

Fig. 4. (**A**) Collision-energy dependence of the differential reactive scattering cross sections, in the backward direction, summed over product vibrational and rotational levels, for the Cl/Cl* + *p*-H_2 reactions for $4 \leq E_c \leq 6$ kcal/mol. The squares and circles are the experimental data, and the lines display the theoretical results from calculations on the CW set of PESs. (**B**) The ratio of the cross sections shown in (A). The red curve and the green circles indicate, respectively, the results of our theoretical calculations on the CW and XJ PESs, whereas the diamonds indicate the experimental results. The evaluation of the error bars of the experimental data in this figure is discussed in the SOM (*25*).

sion energies at which experiments were done, the experimental Cl/Cl* + H_2 DCSs were scaled to the theoretical CW values by means of a single multiplicative factor.

The reactive backward DCS for the BO-allowed Cl-atom reaction increases much more rapidly with increasing collision energy than that for the BO-forbidden reaction of Cl*. This was the prediction of our earlier scattering calculations (*5*). The energy dependence of the ratio of the backward DCSs for the Cl and Cl* reactions is shown in Fig. 4B. As can be seen, agreement with the predictions of quantum-scattering calculations on both PESs is almost always within the experimental uncertainty limits. Only at the lowest collision energy studied here, ~4.2 kcal/mol, is the excited spin-orbit state more reactive than the ground spin-orbit state.

The excellent overall agreement between our molecular beam experiments and the results of quantum-reactive scattering calculations on two sets of ab initio PESs indicates that the theoretical formulation includes correctly the essential physics governing the nonadiabatic processes of importance in the Cl + H_2 reaction. The degree of agreement, both for this and the F/F*+D_2 reaction (*11*), demonstrates that we can now attain the same level of accuracy in the theoretical modeling of triatomic reactions involving multiple PESs as has been achieved previously for reactions in which only one PES is included (*6*, *10*, *30*, *31*). Ultimately, the success attained here should encourage similarly detailed experimental-theoretical investigations of non-BO effects in more complex chemical reactions (*32*, *33*).

References and Notes

1. T. C. Allison *et al.*, in *Gas-Phase Chemical Reaction Systems: Experiments and Models 100 Years After Max Bodenstein*, J. Wolfrum, H.-R. Volpp, R. Rannacher, J. Warnatz, Eds. (Springer, Heidelberg, Germany, 1996), pp. 111–124.
2. M. Alagia *et al.*, *Science* **273**, 1519 (1996).
3. P. Casavecchia, *Rep. Prog. Phys.* **63**, 355 (2000).
4. K. J. Laidler, *Chemical Kinetics* (Harper and Row, New York, 1987), pp. 14, 288–298.
5. M. H. Alexander, G. Capecchi, H.-J. Werner, *Science* **296**, 715 (2002).
6. D. Skouteris *et al.*, *Science* **286**, 1713 (1999).
7. N. Balucani *et al.*, *Phys. Rev. Lett.* **91**, 013201 (2003).
8. E. Garand, J. Zhou, D. E. Manolopoulos, M. H. Alexander, D. M. Neumark, *Science* **319**, 72 (2008).
9. D. E. Manolopoulos *et al.*, *Science* **262**, 1852 (1993).
10. M. Qiu *et al.*, *Science* **311**, 1440 (2006).
11. L. Che *et al.*, *Science* **317**, 1061 (2007).
12. M. H. Alexander, G. Capecchi, H.-J. Werner, *Faraday Discuss. Chem. Soc.* **127**, 59 (2004).
13. J. M. Bowman, *Science* **319**, 40 (2008).
14. P. J. Dagdigian, M. L. Campbell, *Chem. Rev.* **87**, 1 (1987).
15. G. Li, H.-J. Werner, F. Lique, M. H. Alexander, *J. Chem. Phys.* **127**, 174302 (2007).
16. W. Bian, H.-J. Werner, *J. Chem. Phys.* **112**, 220 (2000).
17. H.-J. Werner, M. Kallay, J. Gauss, *J. Chem. Phys.* **128**, 034305 (2008).
18. S. H. Lee, L.-H. Lai, K. Liu, H. Chang, *J. Chem. Phys.* **110**, 8229 (1999).
19. F. Dong, S.-H. Lee, K. Liu, *J. Chem. Phys.* **115**, 1197 (2001).
20. B. F. Parsons, K. E. Strecker, D. W. Chandler, *Eur. Phys. J.* **38**, 15 (2006).
21. M. H. Alexander, J. Kłos, D. E. Manolopoulos, *J. Chem. Phys.* **128**, 084312 (2008).
22. L. Schnieder, K. Seekamp-Rahn, E. Wrede, K. H. Welge, *J. Chem. Phys.* **107**, 6175 (1997).
23. G. Capecchi, H.-J. Werner, *Phys. Chem. Chem. Phys.* **6**, 4975 (2004).
24. M. Qiu *et al.*, *Rev. Sci. Instrum.* **76**, 083107 (2005).
25. Methods are available as supporting material on *Science* Online. See fig. S1 for the REMPI spectrum of the Cl and Cl* atoms, fig. S2 for a comparison of the lowest CW and JX PES in collinear geometry, and fig. S3 for a comparison of the DCSs predicted by the simulations on the CW and JX PESs.
26. M. H. Alexander, D. E. Manolopoulos, H. J. Werner, *J. Chem. Phys.* **113**, 11084 (2000).
27. M. H. Alexander, Y.-R. Tzeng, D. Skouteris, in *Chemical Reaction Dynamics*, G. Lendvay, A. Laganá, Eds. (Kluwer, Amsterdam, 2004), pp. 45–65.
28. K. Stark, H.-J. Werner, *J. Chem. Phys.* **104**, 6515 (1996).
29. D. Skouteris *et al.*, *J. Chem. Phys.* **114**, 10662 (2001).
30. S. Althorpe *et al.*, *Nature* **416**, 67 (2002).
31. F. J. Aoiz, L. Bañares, V. J. Herrero, *Int. Rev. Phys. Chem.* **24**, 119 (2005).
32. W. Hu, G. Lendvay, B. Maiti, G. C. Schatz, *J. Phys. Chem. A* **112**, 2093 (2008).
33. P. Casavecchia *et al.*, *J. Phys. Chem. A* **109**, 3527 (2005).

34. X.Y. and D.H.Z. were supported by the Chinese Academy of Sciences, the National Natural Science Foundation of China, and the Ministry of Science and Technology of China. D.X. was supported by the National Natural Science Foundation of China (20533060 and 20725312). P.C. is grateful to X.Y. and the Dalian Institute of Chemical Physics for a visiting professorship. H.J.W. is grateful to the German Fonds der Chemischen Industrie for financial support.

Supporting Online Material

www.sciencemag.org/cgi/content/full/322/5901/573/DC1
Materials and Methods
Figs. S1 to S3
References

14 July 2008; accepted 19 September 2008
10.1126/science.1163195

Midbody Targeting of the ESCRT Machinery by a Noncanonical Coiled Coil in CEP55

Hyung Ho Lee,[1] Natalie Elia,[2] Rodolfo Ghirlando,[1] Jennifer Lippincott-Schwartz,[2] James H. Hurley[1]*

The ESCRT (endosomal sorting complex required for transport) machinery is required for the scission of membrane necks in processes including the budding of HIV-1 and cytokinesis. An essential step in cytokinesis is recruitment of the ESCRT-I complex and the ESCRT-associated protein ALIX to the midbody (the structure that tethers two daughter cells) by the protein CEP55. Biochemical experiments show that peptides from ALIX and the ESCRT-I subunit TSG101 compete for binding to the ESCRT- and ALIX-binding region (EABR) of CEP55. We solved the crystal structure of EABR bound to an ALIX peptide at a resolution of 2.0 angstroms. The structure shows that EABR forms an aberrant dimeric parallel coiled coil. Bulky and charged residues at the interface of the two central heptad repeats create asymmetry and a single binding site for an ALIX or TSG101 peptide. Both ALIX and ESCRT-I are required for cytokinesis, which suggests that multiple CEP55 dimers are required for function.

Cytokinesis, the division of the cytoplasm, is the final step of the M phase of the cell cycle. Cytokinesis begins with the formation of the contractile ring, which drives the growth of the cleavage furrow. Vesicle trafficking components, including the exocyst complex and SNAREs (soluble *N*-ethylmaleimide–sensitive factor attachment protein receptors), deliver the additional membrane needed for the cleavage furrow to grow (*1*–*3*). When the extension of the furrow ends, the contractile ring disassembles, and a structure known as the midbody remains as the final tether between the two daughter cells. The last step in cytokinesis, the cleavage of the plasma membrane at the midbody, is referred to as abscission. The mechanism of abscission became clearer with the discovery that the midbody protein CEP55 (*4*–*6*) recruits two key components of the ESCRT machinery (*7*–*11*): the ESCRT-I complex and ALIX (*12*, *13*). The role of ALIX and ESCRT-I in abscission appears to be recruitment of ESCRT-III subunits, which are required for normal midbody morphology (*14*) and are widely believed to have a membrane scission activity (*15*).

Deletion analysis of ALIX mapped the interaction with CEP55 to a putative unstructured Pro-rich sequence near its C terminus (*12*, *13*). Similarly, the TSG101 subunit of ESCRT-I interacts via an unstructured linker between its ubiquitin-binding UEV domain and the region that forms the core complex with other ESCRT-I subunits (*12*, *13*). CEP55 is a predominantly coiled-coil protein that otherwise lacks familiar protein-protein interaction domains. The predicted coiled coil of CEP55 is interrupted near the middle by a ~60-residue region that has been suggested to serve as a hinge between the N- and C-terminal coiled-coil regions (*13*). Remarkably, this putative hinge region is also the locus for binding to the putative unstructured Pro-rich regions of ALIX and TSG101. Because it is very unusual for two unstructured regions from two different proteins to drive spe-

[1]Laboratory of Molecular Biology, National Institute of Diabetes and Digestive and Kidney Diseases, Bethesda, MD 20892, USA. [2]Cell Biology and Metabolism Branch, National Institute of Child Health and Human Development, Bethesda, MD 20892, USA.

*To whom correspondence should be addressed. E-mail: hurley@helix.nih.gov

Science

The Extent of Non–Born-Oppenheimer Coupling in the Reaction of Cl(^2P) with *para*-H_2

Xingan Wang, Wenrui Dong, Chunlei Xiao, Li Che, Zefeng Ren, Dongxu Dai, Xiuyan Wang, Piergiorgio Casavecchia, Xueming Yang, Bin Jiang, Daiqian Xie, Zhigang Sun, Soo-Y. Lee, Dong H. Zhang, Hans-Joachim Werner and Millard H. Alexander

Science **322** (5901), 573-576.
DOI: 10.1126/science.1163195